JOURNAL OF GEOPHYSICAL RESEARCH, VOL. 96, NO. B7, PAGES 12,193–12,200, JULY 10, 1991

The Rayleigh-Taylor Instability of an Embedded Layer of Low-Viscosity Fluid

WILLIAM S. D. WILCOCK

MIT-WHOI Joint Program in Oceanography Cambridge, Massachusetts

J. A. WHITEHEAD

Department of Physical Oceanography, Woods Hole Oceanographic Institution, Woods Hole, Massachusetts

The properties of gravitational instabilities formed within two-layer fluid systems are well known and have been applied to a variety of geophysical problems. We present theoretical and experimental results for the gravitational instability developed by a three-layer system, comprising a thin low-viscosity low-density fluid layer sandwiched between two thick layers of equal properties. Linearized equations can be used to solve for the initial growth rates as a function of perturbation wavelength. As is the case for two-layer systems, the results yield a fastest growing wavelength, termed the characteristic wavelength, whose value is much greater than the thickness of the low-viscosity layer. The experimental results confirm the ability of the linearized equations to predict the dominant wavelength of the instability. However, for very thin layers or smaller viscosity ratios a second instability is also observed at a scale much greater than the characteristic wavelength. Numerical solutions show that the wavelength of this instability matches that of a fast growing but short-lived mode arising from perturbations which predominantly involve thickening rather than translation of the buoyant layer. The analytical solution also shows that at the characteristic wavelength, the displacement of the lower interface will be initially a factor $2 - \sqrt{3} = 0.268$ that of the upper interface. As the instability develops the characteristic diapir structures, the experiments show that the relative magnitude of these displacements increase, with underlying fluid being drawn up into the head of the diapir.

INTRODUCTION

When a body of fluid underlies a denser fluid a gravitational instability results, which in the particular case that the two fluids are separated by a horizontal boundary is commonly termed a Rayleigh-Taylor instability. The theoretical and experimentally determined properties of such instabilities have been used to model a number of geophysical processes. These include the formation and distribution of salt domes [e.g., *Nettleton*, 1934; *Selig*, 1965; *Biot and Ode*, 1965; *Woidt*, 1978], the emplacement of gneissic domes and granitic batholiths [*Fletcher*, 1972], the initiation of instabilities deep within the mantle [*Ramberg*, 1972; *Whitehead and Luther*, 1975], and the temporal and spatial periodicity of volcanic activity in a variety of geological settings, namely, island arcs [*Marsh and Carmicheal*, 1974; *Fedotov*, 1975; *Marsh*, 1979], continental rifts [*Mohr and Wood*, 1976; *Bonatti*, 1985], Iceland [*Sigurdsson and Sparks*, 1978], and mid-ocean ridges [*Whitehead et al.*, 1984; *Schouten et al.*, 1985; *Crane*, 1985; *Whitehead*, 1986]. Such models, however, have been based largely upon the results of studies that were limited to a simple two-layer configuration. This simple geometry prohibits motion of the lower boundary of the buoyant layer, a constraint that may be particularly unrealistic when the layer is thin. Many of the geophysical processes of interest could be better modelled by the introduction of a gravitationally stable fluid beneath the buoyant layer. In this paper we report both theoretical and experimental results for the instability developed by a three-layer system, comprising a thin layer of buoyant low-viscosity fluid sandwiched between two thick layers of equal properties.

The initial stages of the Rayleigh-Taylor instability may be analyzed theoretically using linearized flow equations. Solutions may be obtained for the growth rate of instabilities as a function of wavelength and were first derived for invisid fluids by *Rayleigh* [1883] and *Taylor* [1950]. *Harrison* [1908] generalized Rayleigh's treatment to include viscous forces, but it was not until *Bellman and Pennington* [1954] and *Chandrasekhar* [1955] that full solutions were obtained. The introduction of viscous terms in the analysis results in a finite-valued fastest growing wavelength termed the characteristic wavelength. Further analytical and numerical solutions have since been obtained for a variety of geophysically relevant two-layer configurations [*Danes*, 1964; *Selig*, 1965; *Biot and Ode*, 1965; *Biot*, 1966; *Ramberg*, 1968*a*; *Artyushkov*, 1971; *Berner et al.*, 1972; *Whitehead and Luther*, 1975; *Turcotte and Schubert*, 1982]. Inspection of nonlinear terms suggests that as an instability develops, the relative growth rate at the characteristic wavelength might be expected to increase [*Danes*, 1964; *Whitehead and Luther*, 1975]. Thus it is generally assumed that the characteristic wavelength will become the dominant wavelength in the later stages of the instability, though finite element models [*Schmeling*, 1987] show that this may not be the case when the initial perturbation is dominated by wavelengths longer than the characteristic wavelength. The theoretical two-layer studies have been complimented by a large number of experimental studies using a variety of materials with both Newtonian [e.g., *Nettleton* 1934, 1943; *Ramberg*, 1967; *Berner et al.*, 1972; *Whitehead and Luther*, 1975; *Whitehead*, 1986] and non-Newtonian properties [e.g., *Parker and McDowell*, 1951, 1955; *Ramberg*, 1967, 1968*b*, 1972; *Tanner and Williams*, 1968; *Dixon*, 1975]. These experiments confirm the ability of the linearized theory to predict initial

Paper number 91JB00339.
0148-0227/91/91JB-00339$05.00

growth rates and the dominant wavelength. The characteristic diapir structures observed in the later stages of the instability are in good agreement with the results of finite element models [*Berner et al.*, 1972; *Woidt*, 1978].

In contrast to the exhaustive work conducted on two-layer systems, studies of more complex geometries have been limited. *Ramberg* [1968c] developed a numerical model for studying multilayered systems. More recently, *Lister and Kerr* [1989] presented analytical solutions for a buoyant layer sandwiched between two half-spaces and for a horizontal cylinder. In this paper we present analytical and experimental results for a buoyant low-viscosity layer sandwiched between two thick layers. Our analytical solution differs from the more general solution of *Lister and Kerr* [1989] in that the relative amplitude of the perturbations applied at the two interfaces is treated as an unknown, an approach that is necessary to explain more fully the experimental results. *Ramberg* [1972] also studied similar three-layer configurations. However, the numerical results that he presents are not fully in accord with our analytical solution, and the experimental work was confined to non-Newtonian materials with little contrast in viscous properties between layers.

AN ANALYTICAL SOLUTION FOR A LOW-VISCOSITY LAYER

This section is concerned with the analytical solution of the simple three-layer geometry shown in Figure 1 . This comprises a central layer of thickness $h(= 2d)$, sandwiched between two equal half-spaces of higher density ($\rho 1 = \rho 3 > \rho 2$) and considerably higher viscosity ($\mu 1 = \mu 3 \gg \mu 2$).

The viscous flow within each fluid layer can be described by the incompressibility condition:

$$\nabla \cdot \mathbf{u} = 0 \tag{1}$$

and the linearized Navier-Stokes equation:

$$\left(\frac{\partial}{\partial t} - \nu\nabla^2\right) \mathbf{u} = -\left(\frac{1}{\rho}\right) \nabla P \tag{2}$$

where u is the velocity, ν is the kinematic viscosity, ρ is the density, and P is the deviatoric pressure. Equations (1) and (2) may be combined [*Chandrasekhar*, 1955] to give

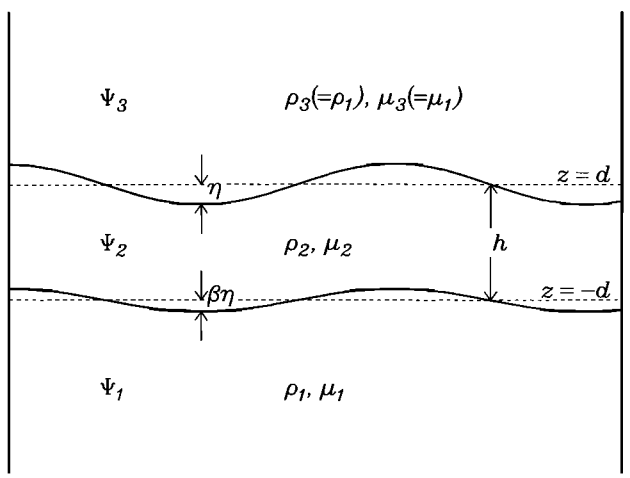

Fig. 1. Sketch showing the configuration of the three-layer system described in the text for which an analytical solution is obtained.

$$\left(\frac{\partial}{\partial t} - \nu\nabla^2\right) \nabla^2\Psi = 0 \tag{3}$$

where Ψ is the stream function defined by

$$\mathbf{u} = \nabla \times \Psi\hat{\mathbf{k}} \tag{4}$$

in two dimensions or the vertical component of velocity in three dimensions.

Dimensional analysis yields a criterion for slow viscous flow:

$$\frac{gh^3\Delta\rho}{\nu^2\rho} \ll 1 \tag{5}$$

where g is the gravitational constant, h is the layer thickness, $\Delta\rho$ is the density contrast between layers, and ρ is the density of the layer. Since this condition is generally satisfied by geophysical processes, the inertial terms may be dropped from (3) which reduces to

$$\nabla^4\Psi = 0 \tag{6}$$

A periodic solution within each layer is

$$\Psi_i = (A_i e^{-kz} + B_i z e^{-kz} + C_i e^{+kz} + D_i z e^{+kz})\, e^{i\mathbf{k}\cdot\mathbf{x}+nt} \tag{7}$$

where k is the horizontal wave number, n is the exponential growth rate constant, and A_i, B_i, C_i, and D_i are unknowns. The necessity for finite flow eliminates two of the exponential terms from (7) in the outer layers. The remaining eight unknowns are determined by the requirement for continuity of vertical and horizontal velocity and of horizontal and vertical stress at the interfaces which for small perturbations may be linearized and written

$$\Psi_i = \Psi_{i+1} \tag{8a}$$

$$D\Psi_i = D\Psi_{i+1} \tag{8b}$$

$$\mu_i \left(D^2 + k^2\right) \Psi_i = \mu_{i+1} \left(D^2 + k^2\right) \Psi_{i+1} \tag{8c}$$

$$\mu_i \left(-D^2 + 3k^2\right) D\Psi_i = \mu_{i+1} \left(-D^2 + 3k^2\right) D\Psi_{i+1} + k^2(\rho_{i+1} - \rho_i) g\eta_i \tag{8d}$$

where $i = 1$ and $i = 2$ correspond to the lower and upper interfaces, respectively, D is $\partial/\partial z$, and η_i is the amplitude of the interface perturbation.

In the analysis of *Lister and Kerr* [1989] the term η_i is replaced by Ψ_i/n, which assumes that the interface perturbation is proportional to the growth rate. In this analysis we assume that the magnitudes of the initial lower and upper interface perturbations have a ratio β. The solution of *Lister and Kerr* [1989] may then be recovered by equating this value to the ratio of interface growth rates α.

To solve the equations, we assume $kd \ll 1$ and approximate $e^{\pm kd}$ by its first-order Taylor expansion $1 \pm kd$, an approximation that can be shown subsequently to be valid for the fastest growing wavelength provided the viscosity ratio $\epsilon = \mu_1/\mu_2$ is at least 10. The flow in the middle layer may then be expressed

$$\begin{bmatrix} kX & -(1-\kappa)X & k & (1+\kappa) \\ k & -(1+\kappa)X & kX & (1-\kappa)X \\ -X & -dX & 1 & d \\ -1 & d & X & -dX \end{bmatrix} \begin{bmatrix} A_2 \\ B_2 \\ C_2 \\ D_2 \end{bmatrix} = \begin{bmatrix} 0 \\ 0 \\ G \\ \beta G \end{bmatrix} \tag{9}$$

where

$$\kappa = kh$$

$$X = (1-\kappa)(1-\epsilon)/(1+\kappa)(1+\epsilon)$$

$$G = (\rho_1 - \rho_2)g\eta/2k^2\mu_2(1+\kappa)(1+\epsilon)$$

To first order in k, the solution is

$$A_2 = G(m_1 + \beta m_2)/m_5 \tag{10a}$$

$$B_2 = kG(-m_3 + \beta m_4)/m_5 \tag{10b}$$

$$C_2 = G(-m_2 - \beta m_1)/m_5 \tag{10c}$$

$$D_2 = kG(m_4 - \beta m_3)/m_5 \tag{10d}$$

where

$$m_1 = X[(1-X^2) + \kappa(X^2+3)]$$

$$m_2 = (X^2-1) - \kappa(3X^2+1)$$

$$m_3 = X(X^2 - 1 - 4\kappa)$$

$$m_4 = X^2 - 1 - 4\kappa X^2$$

$$m_5 = (1-X^2)^2 - 16\kappa^2 X^2$$

Figure 2 is a plot of the solution for a viscosity ratio $\epsilon = 1000$. Two sets of curves are drawn to show the wavelength dependence of the growth rate for fixed ratios of interface perturbations β and growth rate α. The bold line corresponds to the equilibrium growth mode for which $\beta = \alpha$. Inspection of Figure 2 shows that for a given wavelength the growth rate increases as α increases and β decreases. Thus any system initially perturbed in such a way that it does not fall on the equilibrium curve will deform in a way so as to evolve toward it. At long wavelengths it is apparent that nonequilibrium modes with smaller β values than the equilibrium growth mode will initially grow very rapidly with growth rates that may exceed that of the characteristic wavelength. The apparent tendency for these growth rates to continue increasing indefinitely with wavelength results from the failure to include inertial terms in the solution. In practice, the growth rates will be limited by either the inertial length scale or the finite thickness of the confining layers.

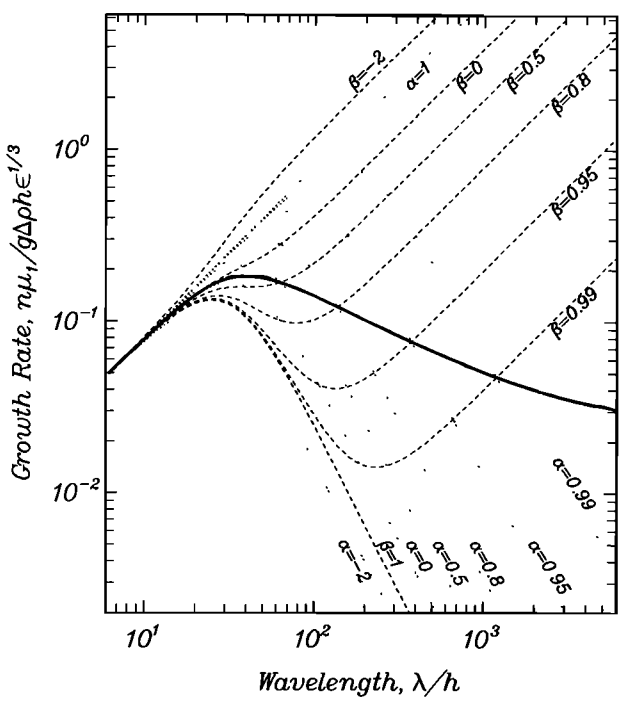

Fig. 2. Growth rate as a function of wavelength for the analytical solution assuming a viscosity contrast $\epsilon = 1000$. Constant ratios of lower to upper interface displacements β and growth rates are shown as dashed and dotted lines, respectively. The solid line is the equilibrium curve for which $\alpha = \beta$. Any system initially perturbed so as to lie off this curve will evolve toward it.

Inspection of β values along the equilibrium curve shows that at smaller wavelengths the lower and upper interfaces are uncoupled. Since the lower interface is stabilizing, any perturbations in it flatten out. As the wavelength increases the flow associated with the deformation of the upper interface penetrates further from the interface and viscous forces couple the motions of the two interfaces. The lower and upper interfaces move together with the stabilizing density stratification across the lower interface acting so as to decrease the rate of growth.

At large values of ϵ it can be shown that the fastest growing equilibrium mode has a characteristic wavelength λ given by

$$k = \frac{2^{2/3}}{h}\,\epsilon^{-1/3}, \qquad \frac{\lambda}{h} = \pi(2\epsilon)^{1/3} \tag{11}$$

The corresponding exponential growth constant is

$$n = \frac{1}{3^{1/2}\,2^{5/3}}\,\frac{g\Delta\rho h}{\mu_1}\,\epsilon^{1/3} \tag{12}$$

and the equilibrium ratio of interface perturbations at the characteristic wavelength is

$$\beta = \alpha = 2 - \sqrt{3} = 0.2679 \tag{13}$$

These results differ from the numerical solutions presented by *Ramberg* [1972]. At large viscosity ratios his results do not very accurately match the characteristic wavelength predicted by (11). Moreover, his results lead him to suggest that the equilibrium value of β decreases indefinitely with increasing viscosity ratio rather than attaining the fixed value defined by (13).

EXPERIMENTAL RESULTS

Experiments were conducted to study the instability developed within a thin horizontal layer of buoyant syrup-water mixture embedded in a medium of pure syrup; the viscous properties of these fluids having been previously shown to be Newtonian. The layer is emplaced by dragging a squared U-shaped tube with a wide (30 cm) horizontal base through a 50×40×15 cm tank filled with syrup. A dyed syrup-water mixture is injected out of finely spaced holes on the front of the tube. The mixture flows around the tube merging into a single sheet in its wake. A mirror angled at 45° beneath the tank allows side and plan view photographs of the developing instability to be taken simultaneously. The experiment was repeated for a variety of layer thicknesses and viscosity contrasts.

The principal drawback of this experimental configura-

tion is that there may be significant local variations in the thickness of the injected layer, the magnitudes of which are difficult to quantify. Experimental considerations suggest that such variations will be primarily orientated perpendicular and parallel to the plane of the U tube. Those in the perpendicular direction can be largely eliminated by dragging the U tube at a constant speed, which for the experiments reported here was achieved by the use of a stepping motor. To avoid a consistent thinning of the layer between the edges and the center, the U tube diameter was chosen large enough that there is no significant drop in flow pressure along its base. The most important cause of unevenness in these experiments results from the finite hole separation which produces small scale thickness variations aligned parallel to the base of the U tube. For these experiments the hole separation (2 mm) was chosen to be significantly smaller than the characteristic wavelengths predicted by the linear theory, and no instabilities were observed at this small a scale in the experiments. Moreover, finite element calculations by *Schmeling* [1987] for a two-layer system show that dominant wavelengths differing significantly from the characteristic wavelength may result only from an uneven distribution of of perturbations dominated by wavelengths greater than the characteristic wavelength. Thus the initial variations in the thickness of the buoyant layer are not expected to affect the dominant wavelength, though they probably cause a consistent orientation of instabilities observed in the experiments.

Figure 3 shows the instability formed by a 0.18 ± 0.02-cm-thick layer centered in 10 cm of syrup with a viscosity ratio of 350 ± 50. The instability forms first in a direction parallel to the U tube, an orientation that coincides with the primary cause of layer unevenness. The noticably earlier development of the instability on the righthand side of the tank results from the finite time (about 1 minute) required to emplace the layer. The final wavelength is 4.0 ± 0.5 cm, a value in good agreement with the predictions of linearized theory (equation 11). The instability in the perpendicular direction develops more slowly and has a slightly greater wavelength (5.0 ± 0.5 cm). This is presumably because the instability in the second direction forms on the thickened crests of the earlier developing instability.

As the instability develops, the regions of upwelling progressively narrow. Marginal differences in growth rates between adjacent upwelling regions are magnified because the fastest growing instabilities are able to drain fluid from neighboring regions. Eventually, characteristic diapir structures [*Whitehead and Luther*, 1975] are formed, consisting of a bulbous head fed by a narrow neck whose dimensions are much smaller than the diapiric separation. Adjacent diapirs are connected by faint spoke-like structures which are the manifestations of ridge structures in the buoyant layer which feed the diminishing supply of fluid into the diapirs.

The linearized theory predicts the lower interface displacement initially will be about one quarter that at the upper interface (equation 13). Inspection of Figure 3 clearly shows that the relative magnitude of such displacements increase as nonlinear terms become important. The side views of the later stages show that the necks of diapirs are primarily composed of a core of fluid from the lower layer. The final frame was taken at a stage when most of the buoyant fluid had reached the surface. In most cases, fluid from below has reached the surface to form a plug in the center of the diapir. This indicates that the lower layer had been drawn up to the base of the diapir head. However, in a few of the larger diapirs the underlying fluid forms an annulus. This

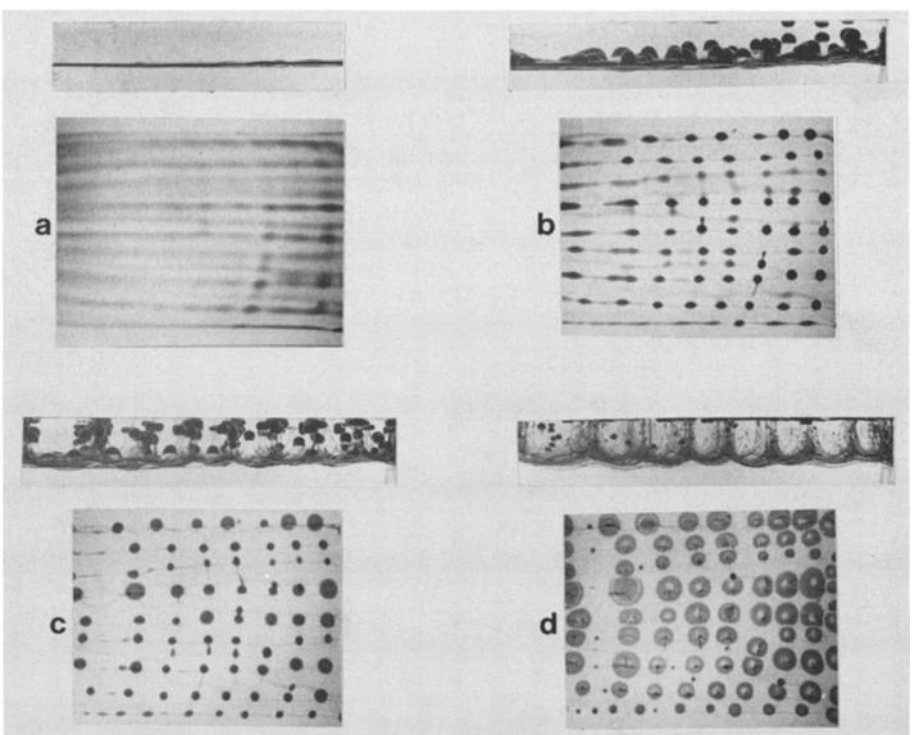

Fig. 3. Photographs recording the development of an instability by a 0.18-cm-thick (± 0.02 cm) layer of a syrup-water mixture centered in 10 cm of syrup. The density contrast $\Delta\rho = 0.1$ g cm^{-3} and the viscosity ratio $\epsilon = 350 \pm 50$. Photographs are for times (*a*) 3:00, (*b*) 6:00, (*c*) 9:00, and (*d*) 18:00 min after emplacement of the buoyant layer. For each frame a side view with dimensions 45×7 cm is shown above a plan-view with dimensions 45×37 cm.

shows that fluid from the lower layer has been entrained into the diapir head and subjected to the characteristic circulatory flow [*Batchelor*, 1963]. A similar experiment conducted for a buoyant layer emplaced at a greater depth suggests that fluid from the underlying layer will eventually be incorporated into the heads of all diapirs.

Figure 4 shows the results for a layer with the same viscosity as the previous example but with a thickness of 0.03 ± 0.005 cm, nearly an order of magnitude thinner than the previous example. Not only is the time scale of the instability significantly longer as is to be expected but the style of deformation is different, showing a bimodal distribution of wavelengths. As for the thicker layer an early instability initially forms parallel to the U tube. The wavelength is about 0.8 ± 0.2 cm, a value similar to that predicted by the linear theory. However, there is also significant deformation at a much longer wavelengths. A second long instability with a wavelength of 10–15 cm is clearly visible on side views but since it involves only a small degree of thickening, it is not readily apparent on plan views. The formation of well-developed diapirs by the first instability only occurs after considerable displacement of the layer and coincides spatially with upwelling regions of the second instability. By this stage the surface of the layer has a very complex shape including significant displacements at a range of intermediate wavelengths. The final separation of diapirs, especially in the direction perpendicular to the U tube, is significantly greater than predicted by the linear theory, a discrepancy that may be attributable to a number of causes other than shortcomings in the theory. As postulated above, the asynchronous development of the short-wavelength instability in two orthogonal directions may result in a longer wavelength in the second direction. Similarly, since the diapirs form on the crests of the long-wavelength instability any thickening that has occurred in these regions may contribute to the larger spacing. Finally, on the time scale of this experiment, diffusive thickening of the layer may be a significant factor.

Figures 5 and 6 summarize the principal wavelengths of deformation observed in two sets of experiments. In Figure 5 the observed wavelengths of instabilities are plotted against the thickness of the buoyant layer for constant viscosity ratio ($\epsilon = 350 \pm 50$), while Figure 6 shows a more limited set of experiments conducted for variable viscosity ratio and constant layer thickness ($h = 0.12 \pm 0.02$ cm). For smaller viscosity ratios or layer thicknesses, a bimodal instability develops with the smaller wavelength matching the characteristic wavelength predicted by the analytical model. A thicker layer or a larger viscosity contrast results in a single instability in good agreement with the linearized theory.

NUMERICAL SOLUTIONS

A qualitative understanding of the differences between the two styles of deformation observed early in the experi-

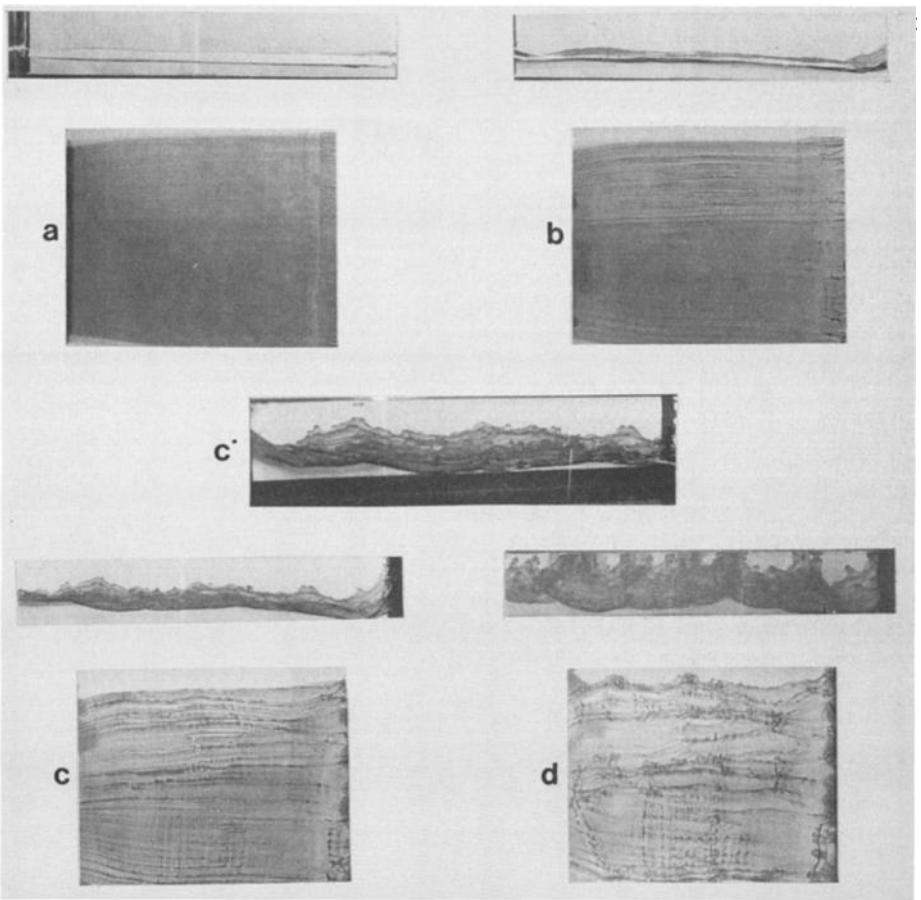

Fig. 4. Photographs recording the development of an instability in a system the same as that of Figure 3, except the layer thickness is 0.03 ± 0.005 cm. Photographs are for times (*a*) 2:00, (*b*) 40:00, (*c*, *c'*) 80:00, and (*d*) 120:00 min. For each frame a side view with dimensions 45×7 cm is shown above a plan-view with dimensions 45×37 cm. The dimensions of side and plan views are 40×7 cm and 40×32 cm, respectively. Figure 4 *c'* is a side view taken at an angle of 45° to Figure 4 *c*, an orientation that shows more clearly the long-wavelength component of deformation.

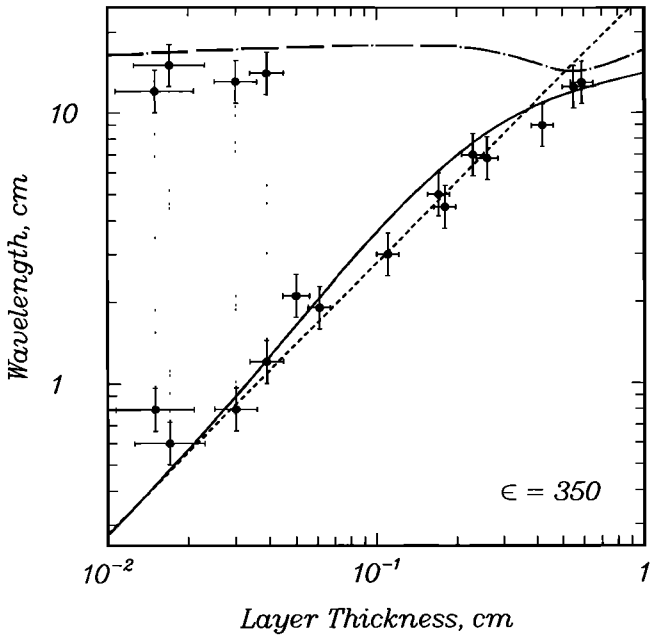

Fig. 5. Experimental observations and linearized predictions of dominant wavelengths as a function of layer thickness for a system comprising a syrup-water layer centered in 10 cm of syrup, with a viscosity ratio $\epsilon = 350 \pm 50$. Experimental results are shown as solid circles together with estimates of uncertainties. Where the wavelength varies with orientation, the value in the direction that forms first is assumed. Dotted lines connect observations from experiments exhibiting a bimodal wavelength instability. Characteristic wavelengths predicted by the numerical model and by equation (11) are shown as solid and dashed lines, respectively. The dot-dashed line shows the wavelength of maximum growth rates for the $\beta = 0$ curve of the numerical model.

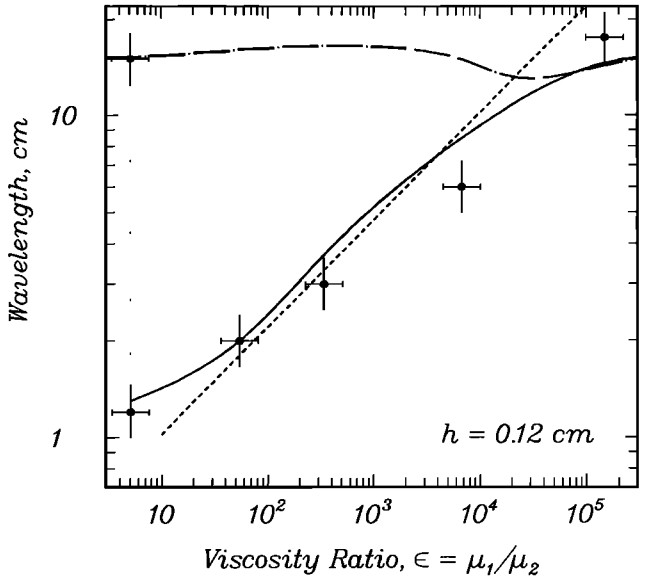

Fig. 6. Experimental observations and linearized predictions of wavelengths of instabilities as a function of viscosity ratio ϵ for a fixed layer thickness of 0.12 ± 0.02 cm plotted using the same conventions as Figure 5.

ments can be obtained by numerically solving a linearized formulation similar to that presented earlier, except that the outer layers are ascribed a finite thickness using appropriate boundary conditions. Figures 7 and 8 show two solutions for configurations that correspond closely to the experiments shown in Figure 3 and 4, respectively.

For the thinner 0.025-cm-thick layer (Figure 8), the characteristic wavelength is virtually that predicted by the analytical model. However, at long wavelengths there are nonequilibrium modes, with low b values, growing up to 10 times more quickly than the characteristic wavelength. At such wavelengths the motions of the two interfaces are strongly coupled and flow extends throughout the system. The middle layer serves to provide the buoyancy driving the instability, while the viscous properties and thicknesses of the outer layers control the style of deformation. The fastest growing nonequilibrium wavelength can be predicted by considering a two-layer problem with layers of equal thickness and viscosity. Such a solution has been derived by *Turcotte and Schubert* [1982] for no-slip boundary conditions, yielding a characteristic wavelength:

$$\lambda = 2.568b \qquad (14)$$

where b is the layer thickness. This solution predicts a wavelength of 12.8 cm in reasonable agreement with Figure 8.

The wavelength of this nonequilibrium mode corresponds closely to the second long-wavelength instability observed in the corresponding experiment (Figure 4). A perturbation at this wavelength which involves a local thickening of the layer will initially grow very rapidly. While the mode will always evolve to the much slower growing equilibrium curve with high b values, there may be a significant amplification of the perturbation in the process. A crude integration down Figure 8 predicts that there will be more than a tenfold amplification of a $\beta = 0$ perturbation before its growth rate no longer exceeds that of the characteristic wavelength. Moreover, the integration predicts only a small change in the layer

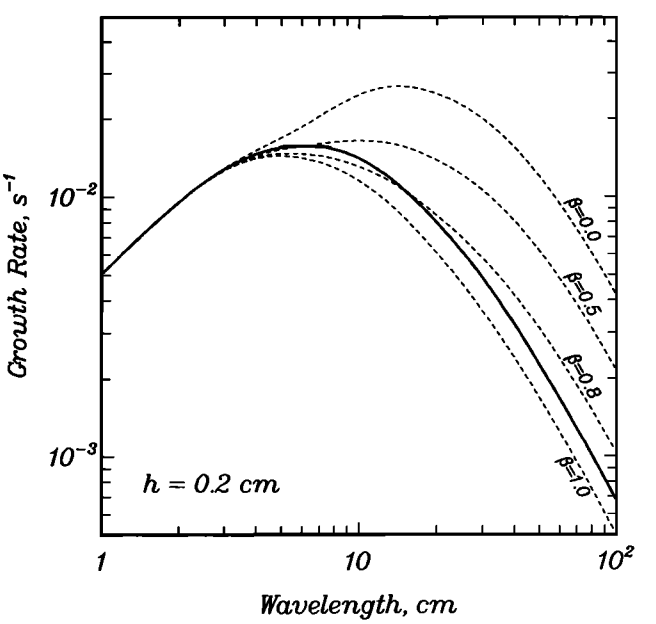

Fig. 7. Numerical solution for the exponential growth rate constant as a function of wavelength for a three-layer configuration similar to that of the experiment shown in Figure 3. Constant β curves are shown as dashed lines, and the equilibrium solution is shown as a solid line.

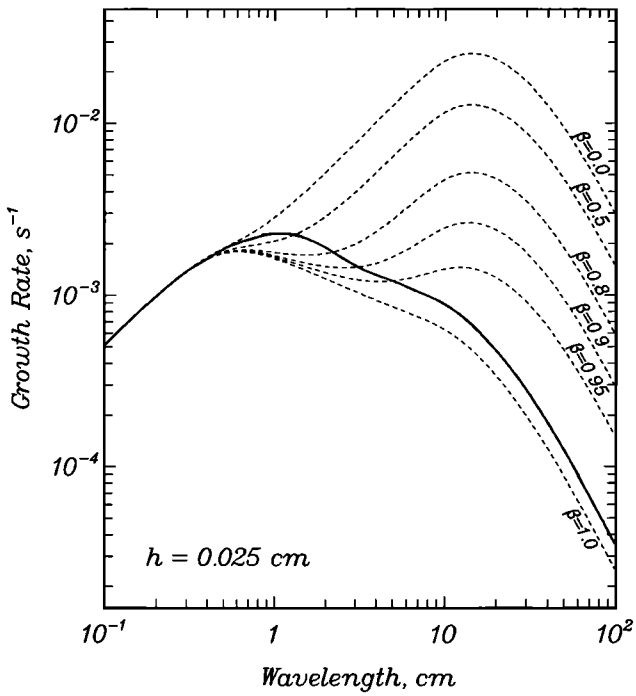

Fig. 8. As for Figure 7 except the configuration is similar to that of the experiment shown in Figure 4.

thickness, in good agreement with the experimental observations. The presence of fast growing nonequilibrium modes also flattens the equilibrium growth curve which shows only a threefold decrease in growth rates at wavelengths ten times the characteristic wavelength. This may explain the experimental observation of significant deformation at a range of intermediate wavelengths (Figure 4).

For the 0.2-cm-thick layer (Figure 7), the maxima in the equilibrium curve is more pronounced. A nonequilibrium mode is still apparent, but since its properties are largely unchanged from Figure 8, while the growth rate and and wavelength of the characteristic wavelength have both increased substantially, it is not as prominent. The growth rate of the nonequilibrium mode for $\beta = 0$ is less than 3 times that of the characteristic wavelength. Such features can explain qualitatively the simpler style of deformation observed in Figure 3.

Ramberg [1967] suggests that the linearized formulation maybe considered valid provided the amplitude of the instability is less than 10% of the wavelength. However, for a three-layer problem the linearized equations are also only accurate while neither interface has broken the initial plane of the other, after which the buoyancy predicted by (8*d*) will be too large. For thin buoyant layers in which the criterion is rapidly violated, the linearized equations might be expected to predict too fast a growth rate. A comparison of Figures 3 and 4 shows that the difference in growth rates appears significantly greater than the factor of 6.0 ± 1.2 predicted by (12), but since the initial interface perturbations are not known in these experiments, a more quantitative comparison is not possible. The error in the buoyancy term might also be expected to change the shape of growth rate versus wavelength curves shown in Figures 7 and 8. However, the wavelengths of instabilities predicted by the numerical model, which are shown in Figures 5 and 6, are in reasonable agreement with the experimental observations, suggesting the effect is not large.

DISCUSSION

The experimental results presented in Figures 5 and 6 together with (11) and (14) yield an approximate expression for the criterion for the development of a dual wavelength instability:

$$\frac{b}{h\epsilon^{1/3}} > \sim 10 \qquad \epsilon > 10, b/h \gg 1 \tag{15}$$

where b and h are the thicknesses of the confining and buoyant layers, respectively. To satisfy this criterion requires a relatively small contrast in the viscosities and a large ratio of layer thicknesses. This condition may be met by compositionally or thermally buoyant layers embedded deep within the mantle. Such layers might be expected to show a significant component of deformation at wavelength much greater than the characteristic wavelength. It should be noted that the origin of the dual wavelength instability described in this paper is not the same as that previously proposed for the D'' layer [*Yuen and Peltier*, 1980; *Christensen*, 1984; *Olson et al.*, 1987] since these works considered a two-layer problem for which the shorter-wavelength instability was confined to a thermally growing boundary layer with strongly temperature dependent viscosity.

For problems such as salt dome formation and volcanic periodicity, (15) is probably not satisfied, and the instability developed can be adequately described in terms of a single characteristic wavelength derived from the linearized equations of flow. The wavelength and growth rate of the three-layer analytical solution (equations (11) and (12)) presented above can be compared with two-layer solutions incorporating an infinite upper layer [*Selig*, 1965; *Whitehead and Luther*, 1975; *Lister and Kerr*, 1989]. The solutions follow the same power law dependencies, while the constants of proportionality differ only slightly, those for the three-layer case lying intermediate between two-layer solutions with no slip and free slip at the base of the buoyant layer. Thus it can be concluded that quantitative solutions for characteristic wavelengths and growth rates obtained using a two-layer geometry are not seriously in error because of the failure to use a three-layer model.

However, the use of a three-layer model yields important information about the nature of deformation at the base of the buoyant layer. For the case in which the confining layers have the same properties, (13) predicts displacements of the lower interface initially one quarter those of the upper interface. The experimental results presented above and those of *Ramberg* [1972] for instabilities developing between layers with little viscosity contrast show that in the later stages, fluid from the lower layer reaches up into the neck of the diapir and may mix with the buoyant layer. These observations are in accordance with the deformation observed around a sphere moving through a viscous medium [*Schmeling et al.*, 1988]. As *Ramberg* [1972] points out, such large motions of the lower interface are only energetically feasible when the density of the fluid immediately beneath the buoyant layer does not exceed that of the fluid immediately above. However, numerical solutions for cases which do not satisfy this criterion still show initial displacements of the lower interface.

Applying these results to geophysical problems suggests

that for relatively shallow features such as salt domes and granitic batholiths, anticlinal structures may exist beneath the diapirs. The magnitude of such structures may depend upon the contrast between the properties of the underlying and overlying units. Diapirs which form at large depths and which undergo considerable motion may inevitably incorporate material from underlying regions. If diapirs develop in thermally or chemically buoyant regions deep within the mantle, such a process might have a significant effect on the composition of partial melts derived at a later stage from such features.

Acknowledgments. We thank Robert Frazel for assistance with the construction and conduct of the experiments and for the photography. This work was supported by a grant from Woods Hole Oceanographic Institution's Ocean Ventures Fund and by the National Science Foundation, Experimental and Theoretical Geophysics Section under grant EAR 87-08033. Woods Hole Oceanographic Institution Contribution No. 7612.

REFERENCES

Artyushkov, E. V., Convective instability in geotectonics, *J. Geophys. Res., 76*, 1397–1415, 1971.

Batchelor, G. K., *An Introduction to Fluid Mechanics*, pp. 235–238, Cambridge University Press, New York, 1967.

Bellman, R., and R. H. Pennington, Effects of surface tension and viscosity on Taylor instability, *Q. Appl. Math., 12*, 151–162, 1954.

Berner, H., H. Ramberg, and O. Stephansson, Diapirism in theory and experiment, *Tectonophysics, 15*, 197–218, 1972.

Biot, M. A., Three-dimensional gravity instability derived from two-dimensional solutions, *Geophysics, 31*, 153–166, 1966.

Biot, M. A., and H. Ode, Theory of gravity instability with variable overburden and compaction, *Geophysics, 30*, 213–227, 1965.

Bonatti, E., Punctiform initiation of seafloor spreading in the Red Sea during transition from a continental to an oceanic rift, *Nature, 316*, 33–37, 1985.

Chandrasekhar, S., The character of the equilibrium of an incompressible heavy viscous fluid of variable density, *Proc. Cambridge Philos. Soc., 51*, 162–178, 1955. (Reprinted in *Hydrodynamics and Hydromagnetic Stability*, pp. 441–453, Oxford University Press, New York, 1961).

Christensen, U., Instability of a hot boundary layer and initiation of thermo-chemical plumes, *Ann. Geophys., 2*, 311–320, 1984.

Crane, K., The spacing of rift axis highs: Dependence upon diapiric processes in the underlying asthenosphere?, *Earth Planet. Sci. Lett., 72*, 405–414, 1985.

Danes, Z. F., Mathematical formulation of salt-dome dynamics, *Geophysics, 29*, 414–424, 1964.

Dixon, J. M., Finite strain and progressive deformation in models of diapiric structures, *Tectonophysics, 28*, 89–124, 1975.

Fedotov, S. A., Mechanism of magma ascent and deep feeding channels of island arc volcanoes, *Bull. Volcanol., 39*, 241–254, 1975.

Fletcher, R. C. Application of mathematical model to emplacement of mantled gneiss domes, *Am. J. Sci., 272*, 197–216, 1972.

Harrison, W. J., The influence of viscosity on the oscillations of superposed fluids, *Proc. London Math. Soc., Ser. 2*, 6, 396–405, 1908.

Lister, J. R., and R. C. Kerr, The effect of geometry on the gravitational instability of a buoyant region of viscous fluid, *J. Fluid Mech., 202*, 577–594, 1989.

Marsh, B. D., Island arc development: Some observations and speculations, *J. Geol., 87*, 687–713, 1979.

Marsh, B. D., and I. S. E. Carmichael, Benioff zone magmatism, *J. Geophys. Res., 79*, 1196–1206, 1974.

Mohr, P. A., and C. A. Wood, Volcano spacings and lithospheric attenuation in the eastern rift of Africa, *Earth Planet. Sci. Lett., 33*, 126–144, 1976.

Nettleton, L. L., Fluid Mechanics of salt-domes, *Am. Assoc. Pet. Geol. Bull., 18*, 1175–1204, 1934.

Nettleton, L. L., Recent experimental and geophysical evidence of mechanics of salt-dome formation, *Am. Assoc. Pet. Geol. Bull., 27*, 51–63, 1943.

Olson, P., G. Shubert, and C. Anderson, Plume formation in the D''-layer and the roughness of the core-mantle boundary, *Nature, 327*, 409–413, 1987.

Parker, T. J., and A. N. McDowell, Scale models as a guide to interpretation of salt-dome faulting, *Am. Assoc. Pet. Geol. Bull., 35*, 2076–2086, 1951.

Parker, T. J., and A. N. McDowell, Model studies of salt-dome tectonics, *Am. Assoc. Pet. Geol. Bull., 39*, 2384–2470, 1955.

Ramberg, H., Model experimentation of the effect of gravity on tectonic processes, *Geophys. J. R. Astron. Soc., 14*, 307–329, 1967.

Ramberg, H., Instability of layered systems in the field of gravity, 2, *Phys. Earth Planet. Inter., 1*, 448–474, 1968*a*.

Ramberg, H., Fluid dynamics of layered systems in the field of gravity, a theoretical basis for certain global structures and isostatic adjustment, *Phys. Earth Planet. Inter., 1*, 63–87, 1968*b*.

Ramberg, H., Instability of layered systems in the field of gravity, 1, *Phys. Earth Planet. Inter., 1*, 427–447, 1968*c*.

Ramberg, H., Mantle diapirism and its tectonic and magmagenetic consequences, *Phys. Earth Planet. Inter., 4*, 45–60, 1972.

Rayleigh, Lord (J. W. Strutt), Investigations of the character of an incompressible heavy fluid of variable density, , *Proc. London Math. Soc., 14*, 170–177, 1883. (Reprinted in *Scientific Papers by Lord Rayleigh, 2*, pp. 200–207, Dover, New York, 1964.)

Schmeling, H., On the relation between initial conditions and late stages of Rayleigh-Taylor instabilities, *Tectonophysics, 133*, 65–80, 1987.

Schmeling, H., A. R. Cruden, and G. Marquart, Finite deformation in and around a fluid moving through a viscous medium: Implications for diapiric ascent, *Tectonophysics, 149*, 17–34, 1988.

Schouten, H., K. D. Klitgord, and J. A. Whitehead, Segmentation of mid-ocean ridges, *Nature, 317*, 225–229, 1985.

Selig, F., A theoretical prediction of salt-dome patterns, *Geophysics, 30*, 633–645, 1965.

Sigurdsson, H., and S. R. J. Sparks, Lateral magma flow within rifted Icelandic crust, *Nature, 274*, 126–130, 1978.

Tanner, W. F., and G. K. Williams, Model diapirs, plasticity and tension, in Diapirism and Diapirs, edited by J. Braunstein and G. D. O'Brien, *Mem. Am. Assoc. Pet. Geol., 8*, 10–15, 1968.

Taylor, G., The instability of liquid surfaces when accelerated in a direction perpendicular to their planes, 1, *Proc. R. Soc. London, Ser. A, 201*, 192–196, 1950.

Turcotte, D. L., and G. Schubert, *Geodynamics Applications of Continuum Physics to Geological Problems*, pp. 251–257, John Wiley, New York, 1982.

Whitehead, J. A., Buoyancy-driven instabilities of low-viscosity zones as models of magma-rich zones, *J. Geophys. Res., 91*, 9303–9314, 1986.

Whitehead, J. A., and D. S. Luther, Dynamics of laboratory diapir and plume models, *J. Geophys. Res., 80*, 705–717, 1975.

Whitehead, J. A., H. J. B. Dick, and H. Schouten, A mechanism for magmatic accretion under spreading centers, *Nature, 312*, 146–148, 1984.

Woidt, W. D., Finite element calculations applied to salt-domes analysis, *Tectonophysics, 50*, 369–386, 1978.

Yuen, D. A., and W. R. Peltier, Mantle Plumes and the thermal stability of the D'' layer, *Geophys. Res. Lett., 7*, 625–628, 1980.

J. A. Whitehead, Department of Physical Oceanography, Woods Hole Oceanographic Institution, Woods Hole, MA 02543.

W. S. D. Wilcock, Department of Earth, Atmospheric, and Planetary Sciences, Room 54-510, Massachusetts Institute of Technology, Cambridge, MA 02139.

(Received June 15, 1990;
accepted January 3, 1991.)